A Mixed Conduction Mode Control Strategy Based on Fixed Turn-OFF Time for Totem-Pole PFC Converter

Fangang Meng, *Member, IEEE*, Yuan Shu, Jinmeng Wu, *Graduate Student Member, IEEE*, Shengren Yong, and Yufeng Chen

***Abstract*—This article proposes a mixed conduction mode (MCM) control strategy based on a fixed turn-OFF time (FOT) to address the issues of low light-load efficiency, poor power factor, and high current stress in the single-mode operation of the totem-pole power factor correction (PFC) converter. This strategy enables hybrid operation between discontinuous conduction mode (DCM) and continuous conduction mode (CCM) within a half-line cycle. By FOT of the transistor, the switching boundary between DCM and CCM is clearly defined, enabling adaptive mode switching in accordance with output power. Furthermore, a DCM/CCM turn-ON time prediction model has been developed to unify the DCM/CCM control loops, thereby ensuring stable MCM operation. Finally, a 1500-W-rated prototype totem-pole PFC converter has been designed to validate the effectiveness of the control strategy. The experimental results demonstrate that, compared to the ideal critical conduction mode operation, the proposed control strategy effectively reduces the current stress of the converter, and the peak value of the inductance current is reduced by 16.1% at full load. In comparison to the traditional CCM control, the proposed control strategy significantly enhances the light-load performance of the converter, achieving a maximum improvement of 11.6% in light-load efficiency, a 0.295 increase in power factor, and 7.1% decrease in iTHD.**

***Index Terms*—Adaptive switching, fixed turn-OFF time (FOT), mixed conduction mode (MCM), totem-pole power factor correction (PFC) converter.**

I. Introduction

THE totem-pole power factor correction (PFC) converter is a widely used front-end topology for two-stage ac–dc converters in various power supply applications, such as automotive power systems and server power supplies, due to the advantages of fewer components, simpler structures, and lower electromagnetic interference noise [1], [2], [3], [4].

The totem-pole PFC converter can be classified into continuous conduction mode (CCM), critical conduction mode (CRM), and discontinuous conduction mode (DCM) according to the continuity of the inductor current. In CCM, the converter experiences lower current stress, making it suitable for high-power applications. However, under light-load conditions, the converter may enter DCM, which leads to a decrease in performance parameters such as efficiency and power factor [5]. In DCM or CRM, soft switching or valley switching can be achieved to improve efficiency. However, the current stress in these modes is high, limiting their suitability to low-power applications. Additionally, the traditional CRM control strategy may result in excessively high switching frequencies near the input voltage zero-crossing point [6], [7]. To address the limitations of single-mode operation, researchers have proposed the mixed conduction mode (MCM) control strategy, which combines the advantages of single-mode while compensating for its shortcomings.

In recent years, there has been less research on the MCM control strategy for the totem-pole PFC converter. However, the operating principle of the totem-pole PFC converter can be viewed as equivalent to that of the traditional boost PFC. Several MCM control strategies have currently been proposed for the boost PFC, providing a basis for the totem-pole PFC. These strategies can be mainly classified into the following two categories.

The first category does not require additional detection circuits but focuses on optimizing the control strategy to achieve MCM operation. As early as 2005, Gusseme et al. [8] proposed a control scheme that combines sampling correction and duty-cycle feedforward to address input current distortion under light-load DCM operation in the CCM control strategy, thereby enabling MCM operation. In this optimization approach, Lim and Khambadkone [9] proposed a correction factor, and Wang et al. [10] designed an average current estimation circuit to correct the inductor current sampling in DCM mode. Meanwhile, Wang and Tzou [11] addressed the DCM inductor current sampling error by modifying the sampling logic and designing a repetitive controller to reduce current loop error, thus enabling MCM operation. In addition to sampling correction, several novel control strategies have been proposed to achieve MCM operation. Wang and Tzou [12] employed a predictive control strategy that successfully implements MCM operation by adjusting the control approach according to mode changes. Similarly, Nair and Narasamma [13] applied predictive control

Received 13 December 2024; revised 4 March 2025 and 18 April 2025; accepted 2 June 2025. Date of publication 9 June 2025; date of current version 5 August 2025. This work was supported by the Natural Foundation of Shandong Province under Grant ZR2023ME020. Recommended for publication by Associate Editor C. Chen. *(Corresponding author: Fangang Meng.)*

The authors are with the School of Electrical Engineering and Automation, Harbin Institute of Technology, Weihai 264209, China (e-mail: mfg0327@sina.com; 22s130574@stu.hit.edu.cn; 21b906017@stu.hit.edu.cn; 23s130524@stu.hit.edu.cn; 24s030089@stu.hit.edu.cn).

Color versions of one or more figures in this article are available at https://doi.org/10.1109/TPEL.2025.3578152.

Digital Object Identifier 10.1109/TPEL.2025.3578152

TABLE I
EXISTING CONTROL STRATEGIES FOR DIFFERENT MODES

Control strategy / Operating mode	Average current control	Peak current control	LUT control	Predictive control	VOT control	COT control	FOT control
CCM	√	√	×	√	√	×	×
CRM	×	√	√	√	×	√	×
DCM	√	√	√	√	√	√	√
MCM	√	√	√	√	√	×	×

concepts to forecast the operating mode of the next cycle, thereby enabling MCM operation without the need for additional sensors. However, this control strategy is complex. Chen et al. [14] compared the output duty cycles in DCM and CCM to determine the present operating mode, then set the appropriate duty cycle to achieve MCM operation. While this method is easier to implement, it is computationally expensive. Meanwhile, Lai et al. [15] and [16] proposed a strategy to determine the operating mode by calculating the duty cycle, enabling seamless mode switching. Additionally, the mode determination process is simplified through efficient computations.

The above control strategies do not require additional detection circuits, making the hardware design relatively simple. However, most of these strategies were passive compensations or corrections to address the inefficiencies and low power factor problems that occur when traditional CCM control transitions to DCM operation under light-load, and then proposed MCM control. However, most of these control strategies suffer from issues such as complexity, high computational load, and ambiguous mode switching boundaries.

The second category involves adding hardware detection circuits to monitor the converter's present operating mode, thereby selecting the corresponding control strategy to achieve MCM operation. Clark et al. [17] proposed a control strategy that determines the operating mode using a zero-crossing detection (ZCD) circuit and adjusts the compensation parameters within an average current control framework to achieve MCM operation. In contrast, Fernandes and Trescases [18] switched between different control strategies by detecting the peak value of the inductor current, thereby achieving MCM operation. Min et al. [19] combined ZCD with a unified pulsewidth cycle control strategy, enabling MCM operation and valley switching. The addition of detection circuits reduces the computational complexity of the control strategy. However, these approaches use different control methods for different operating mode, requiring multiple control loops, which complicates the overall strategy.

In conclusion, the majority of existing MCM control strategies suffer from inherent issues, such as control complexity and ambiguous mode switching boundaries, regardless of the presence of additional detection circuits. To address the aforementioned issues, this article proposes an MCM control strategy that enables adaptive mode switching for the totem-pole PFC by fixing the turn-OFF time (FOT).

Table I shows the existing control strategies for different modes of the boost PFC and totem-pole PFC. These control strategies are not entirely independent; some can be combined to achieve better control performance, such as the combination of look-up table control and variable ON-time (VOT) control [20].

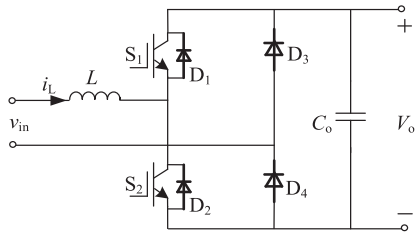

Fig. 1. Topology of the totem-pole PFC converter.

As shown in Table I, the existing FOT control is primarily used for single-mode applications, with limited discussion on its use in MCM operation [21], [22]. By FOT, a DCM/CCM turn-ON time prediction model is established to unify the CCM and DCM control loops, thereby simplifying the overall control strategy. This approach ensures clear and controllable mode-switching boundaries during MCM operation. By combining the advantages of each operating mode, the proposed strategy improves converter performance across a wide load range.

The contributions of this article are summarized as follows:

1) A novel FOT based MCM control strategy for totem-pole PFC converter is proposed, which unifies the control scheme for both CCM and DCM. This integration simplifies the control loop architecture and reduces real-time computational burden.
2) The clear mode switching boundaries are analyzed, and the mode switching can be actively controlled by adjusting the FOT.

The rest of this article is organized as follows. Section II analyzes the fundamental principle of adaptive mode switching based on FOT, establishes the turn-ON time prediction model, and describes the proposed MCM control. Section III discusses the constraints of the FOT, including mode-switching power boundary requirement, peak current limitation, and switching frequency limitation. Section IV validated the accuracy and effectiveness of the proposed MCM control strategy through experiments. Finally, Section V concludes this article.

II. THE PROPOSED MCM CONTROL STRATEGY

Fig. 1 shows the topology of the totem-pole PFC converter. The converter consists of high-frequency switching IGBTs S_1 and S_2, $-D_1$–D_2 as the anti-parallel diodes for the switching IGBTs S_1–S_2, the diodes D_3–D_4, a power inductor L, and an output capacitor C_o, where v_{in} is the input voltage, V_o is the output voltage, and i_L is the current through L.

The principle of the totem-pole PFC converter is similar to that of the boost circuit. Initially, with S_1 turns OFF and S_2 turns ON,

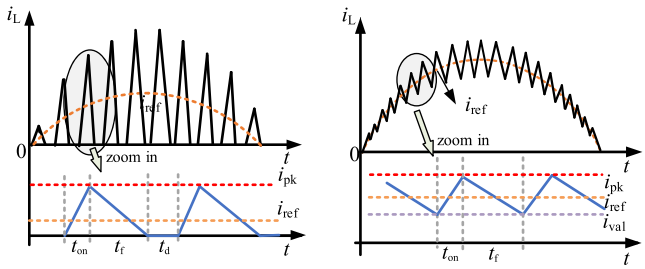

Fig. 2. Current waveform of the totem-pole PFC converter. (a) Ideal DCM. (b) Ideal CCM.

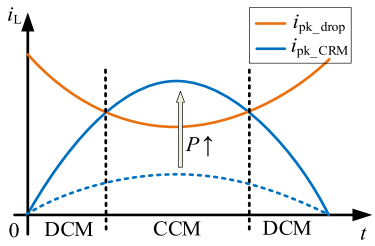

Fig. 3. Relationship between the $i_{\mathrm{pk\_drop}}$ and $i_{\mathrm{pk\_CRM}}$.

the input voltage v_{in} passes through the loop L–S_2–D_4, allowing the inductor to store energy and increasing the inductor current i_L. When S_2 turns OFF, the energy in v_{in} and L flows through D_1 and D_4 to supply power to the load, causing the inductor current to decrease. Repeat the above process until it enters the negative half-line cycle.

A. Adaptive Mode-Switching By FOT

To simplify the analysis, the effects of parasitic parameters are ignored and the inductor current rise and fall are both linear. Fig. 2 shows the current waveform of the totem-pole PFC converter operating in DCM and CCM. The current rise time is defined as t_{ON}, the fall time is t_f, and the time when the inductor current is zero in DCM is t_d. CRM is the boundary of CCM and DCM, which can be regarded as the DCM mode under the condition of $t_d = 0$.

The turn-OFF time t_{OFF} can be expressed as

$$t_{\mathrm{off}} = \begin{cases} t_f, \text{ if CCM} \\ t_f + t_d, \text{DCM.} \end{cases} \tag{1}$$

Once the t_{OFF} is fixed, the peak inductor current drop $i_{\mathrm{pk\_drop}}$ during each half-line cycle in steady state can be expressed as

$$i_{\mathrm{pk\_drop}} = \frac{V_o - |v_{\mathrm{in}}|}{L} t_{\mathrm{off}}. \tag{2}$$

Comparing the peak inductor current with the $i_{\mathrm{pk\_drop}}$, the current operating mode of the totem-pole PFC can be determined. For the PFC converter, the phase of the input current can be approximated to the v_{in}, then the input current reference value i_{ref} is also in phase with the v_{in}, i.e., $i_{\mathrm{ref}} = \mathrm{k}v_{\mathrm{in}}$, where k is a constant. From the basic power equation, the relationship between the i_{ref} and v_{in}, as well as other circuit parameters can be expressed as

$$i_{\mathrm{ref}} = \frac{P_o v_{\mathrm{in}}}{\eta v_{\mathrm{inrms}}^2} \tag{3}$$

where P_o is the output power, η is the converter efficiency, and v_{inrms} is the input voltage rms.

In CRM, the peak value of the inductor current $i_{\mathrm{pk\_CRM}}$ should be twice the i_{ref}, it can be expressed as

$$i_{\mathrm{pk\_CRM}} = 2i_{\mathrm{ref}} = \frac{2P_o v_{\mathrm{in}}}{\eta v_{\mathrm{inrms}}^2}. \tag{4}$$

In combination with (2) to (4), the relationship between the $i_{\mathrm{pk\_drop}}$ and $i_{\mathrm{pk\_CRM}}$ during the positive half-line cycle can be obtained as shown in Fig. 3. There are two cases of the relationship between the $i_{\mathrm{pk\_drop}}$ and $i_{\mathrm{pk\_CRM}}$ with output power variation. At low output power, the $i_{\mathrm{pk\_CRM}}$ is always smaller than the $i_{\mathrm{pk\_drop}}$ in the half-line cycle. The converter operates exclusively in DCM. At high output power, the $i_{\mathrm{pk\_CRM}}$ intersects with the $i_{\mathrm{pk\_drop}}$, and the converter operates in MCM. If $i_{\mathrm{pk\_CRM}} > i_{\mathrm{pk\_drop}}$, the converter operates in CCM; $i_{\mathrm{pk\_CRM}} < i_{\mathrm{pk\_drop}}$, the converter operates in DCM. This enables adaptive switching of operating modes for power conversion by FOT.

In conclusion, the power boundaries between single DCM and MCM of the totem-pole PFC under steady-state conditions can be clarified by FOT. Furthermore, it can simplify the analysis of the converter by FOT, and limited the maximum switching frequency. Thus, the fixed t_{OFF} must be selected judiciously in accordance with the circuit parameters.

B. Turn-on Time Prediction Model

1) DCM Turn-on Time Prediction: After FOT, based on the peak current principle, the turn-ON time prediction models for different modes are established to achieve the PFC function. Fig. 2(a) shows the waveform of inductor current during a positive half-line cycle in DCM. The expression for the peak inductor current i_{pk} during a single switching cycle are as follows:

$$\begin{cases} i_{\mathrm{pk}} = \frac{v_{\mathrm{in}}}{L} t_{\mathrm{on}} \\ i_{\mathrm{pk}} = \frac{V_o - v_{\mathrm{in}}}{L} t_f. \end{cases} \tag{5}$$

In DCM, the relationship between the i_{ref} and i_{pk} can be expressed as

$$i_{\mathrm{ref}} = \frac{i_{\mathrm{pk}}}{2} \frac{t_{\mathrm{on}} + t_f}{t_{\mathrm{on}} + t_{\mathrm{off}}}. \tag{6}$$

In combination with (5) and (6), the expression for the t_{ON} during a single switching cycle in DCM is as follows:

$$t_{\mathrm{on}} = M + \sqrt{M^2 + 2Mt_{\mathrm{off}}} \tag{7}$$

where $M = \frac{Li_{\mathrm{ref}}}{v_{\mathrm{in}}} - \frac{Li_{\mathrm{ref}}}{V_o}$.

2) CCM Turn-on Time Prediction: Fig. 2(b) shows the waveform of inductor current during a positive half-line cycle in CCM. The expression for the peak inductor current i_{pk} during a single switching cycle is as follows:

$$i_{\mathrm{pk}} = 2i_{\mathrm{ref}} - i_{\mathrm{val}} \tag{8}$$

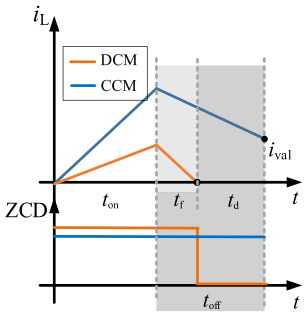

Fig. 4. Current waveforms with ZCD signal.

where the i_{val} is the valley value of the inductor current during a single switching cycle.

In combination with (5) and (8), the expression for the t_{ON} during a single switching cycle in CCM is as follows:

$$t_{on} = \frac{2L\left(i_{ref} - i_{val}\right)}{v_{in}}. \tag{9}$$

C. ZCD of the Inductor Current

In order to enhance the accuracy of mode switching, it is necessary to detect the inductor current ZCD signal within the fixed t_{OFF} to judge the converter operating mode. Fig. 4 shows the current waveforms with ZCD signal in different operating modes. The shaded area represents the FOT stage. If the ZCD signal is present during the t_{OFF}, the totem-pole PFC operates in DCM. In the absence of the ZCD signal, the totem-pole PFC operates in CCM.

In order to enhance the accuracy of mode switching judgment, the anti-false touch design is added to the software, judging three consecutive cycles as the same mode before mode switching, increasing the reliability of the mode switching process.

D. The Proposed MCM Control Strategy

Fig. 5 shows the proposed MCM control scheme. First, the reference value of the inductor current i_{ref} is obtained by the voltage loop controller and digital phase-locked loop. Subsequently, the ZCD signal is generated by sensing the inductor current i_L. The ZCD signal is employed to ascertain the present operating mode, select the corresponding turn-ON time prediction formula, and calculate the switching transistor turn-ON time t_{ON}. The ePWM module of the DSP is used to transform the aforementioned t_{ON} and the fixed t_{OFF} into a PWM signal for driving the high-frequency switches S_1 and S_2. In the positive half-line cycle, S_2 is driven by the output PWM signal; in the negative half-line cycle, S_1 is driven by the output PWM signal.

III. Constraints of the FOT

A. Mode-Switching Power Boundary

Based on the previous analysis, operating in DCM under low power conditions can improve the efficiency of the converter, while operating in MCM under high power conditions can reduce the current stress. The FOT determines the power

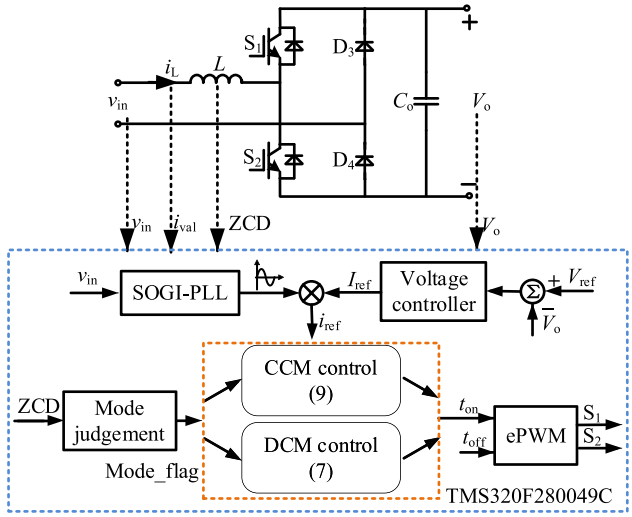

Fig. 5. Proposed MCM control scheme.

boundary for mode switching. Therefore, it is necessary to select an appropriate t_{OFF} for the converter to realize the efficient operation of the converter in a wide load range. The boundary power between single DCM and MCM operation is set as P_{set}, when the output power $P_o < P_{set}$, the converter operates in DCM; when the output power $P_o > P_{set}$, the converter operates in MCM.

To ensure mode switching occurs at the set boundary power, the maximum turn-OFF time in CRM at $P_o = P_{set}$ is selected as one of the constraints for the t_{OFF}. In combination with (4) and (5), the turn-OFF time t_{OFF} in CRM can be expressed as

$$t_{off} = \frac{2i_{ref}L}{V_o - v_{in}}. \tag{10}$$

In combination with (3) and (10), it can be demonstrated that the turn-OFF time t_{OFF} is positively correlated with the v_{in}. When the v_{in} reaches its maximum value v_{inmax}, the t_{OFF} also reaches its maximum value t_{OFFmax}. In order to ensure that the converter operates in single DCM below the P_{set}, the constraint t_1 for the t_{OFF} can be expressed as

$$t_{off} \geq t_1 = t_{offmax} = \frac{2LP_{set}v_{inmax}}{\eta v_{inrms}^2\left(V_o - v_{inmax}\right)}. \tag{11}$$

B. Switching Frequency Limitation

1) Frequency Inversion: The proposed MCM control is a type of frequency modulation control strategy. Conventional frequency modulation control strategies, such as the peak current control for the totem-pole PFC operating in CRM, suffer from an uncontrollable switching frequency. The switching frequency is inversely related to the input voltage amplitude, meaning it increases as the input voltage decreases. Consequently, near the zero-crossing points of the input voltage, the converter may experience excessively high switching frequencies, potentially impacting system stability. Additionally, the high switching frequency leads to increased switching losses and other associated issues.

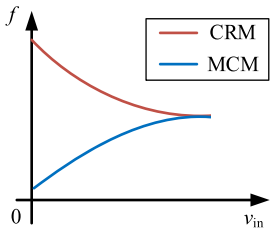

Fig. 6. Frequency inversion.

The proposed MCM control utilizes FOT to limit the switching frequency of the converter while achieving frequency inversion, where the switching frequency is positively correlated with the input voltage. Once FOT, the switching period is inevitably longer than the FOT. This approach effectively addresses the issue of excessively high switching frequencies that may occur in traditional frequency modulation control, thereby enhancing the system's stability.

Fig. 6 shows a comparison of the switching frequency variations between the proposed MCM control and traditional CRM peak current control under the identical conditions. As shown in Fig. 6, the MCM control with FOT can significantly limit the switching frequency of the converter, achieving frequency inversion. In conditions of low input voltage and low power, the lower switching frequency helps reduce switching losses. As the load power and input voltage increase, the rising switching frequency reduces current ripple and current stress, thereby enhancing the system's load capability.

2) Switching Frequency Limitation: In combination with (5) to (9), the expression for the switching frequency f_{CCM} and f_{DCM} of the converter in CCM and DCM can be expressed as

$$\begin{cases} f_{\mathrm{CCM}} = \frac{v_{\mathrm{in}}}{V_o t_{\mathrm{off}}} \\ f_{\mathrm{DCM}} = \frac{M + t_{\mathrm{off}} - \sqrt{M^2 + 2Mt_{\mathrm{off}}}}{t_{\mathrm{off}}^2}. \end{cases} \tag{12}$$

The constraints for the switching frequency f_s are

$$f_{\min} \le f_s \le f_{\max} \tag{13}$$

where $f_{\max}$ is the upper limit of the switching frequency and $f_{\min}$ is the lower limit of the switching frequency.

Take the derivatives of the f_{CCM} and f_{DCM} in (12) with respect to the v_{in} and P_o, respectively. It can be demonstrated that the f_{CCM} and f_{DCM} are monotonically increasing functions with respect to the v_{in} in the operating range, and the switching frequency increases with the increase of the v_{in}. The f_{DCM} is a monotonically decreasing function with respect to the P_o, and the switching frequency decreases with the increase of the output power. In contrast, the f_{CCM} is independent of the P_o. Therefore, it can be concluded that the maximum switching frequency and the minimum switching frequency of the converter in the operating range both occur in DCM. The maximum switching frequency occurs when the P_o is minimum and the v_{in} is maximum; the minimum switching frequency occurs when the P_o is maximum and the v_{in} is minimum. Therefore, the switching frequency constraints can be expressed as

$$\begin{cases} f_{\mathrm{dcm}} \ge f_{\min}, v_{\mathrm{in}} = 0, P_o = P_{\mathrm{omax}} \\ f_{\mathrm{dcm}} \le f_{\max}, v_{\mathrm{in}} = v_{\mathrm{inmax}}, P_o = P_{o\min} \end{cases} \tag{14}$$

where the $P_{o\min}$ is the minimum output power.

In combination with (12) and (14), the constraints t_2 and t_3 for the t_{OFF} can be expressed as

$$\begin{cases} t_{\mathrm{off}} \ge t_2 = \frac{1}{f_{\max}} - \sqrt{\frac{2LP_{o\min}(V_o - v_{\mathrm{inmax}})}{f_{\max}\eta V_o v_{\mathrm{inrms}}^2}} \\ t_{\mathrm{off}} \le t_3 = \frac{1}{f_{\min}} - \sqrt{\frac{2LP_{o\max}}{f_{\min}\eta v_{\mathrm{inrms}}^2}}. \end{cases} \tag{15}$$

C. Peak Current Limitation

For the purpose of ensuring the safe operation of the converter, considering practical parameters such as inductor saturation current and the current-carrying capacity of the switches, it is necessary to limit the peak inductor current. In combination with (2) to (9), the peak inductor current of the totem-pole PFC converter operating in CCM or DCM under FOT can be expressed as

$$\begin{cases} i_{\mathrm{pk\_CCM}} = i_{\mathrm{ref}} + \frac{(V_o - v_{\mathrm{in}})t_{\mathrm{off}}}{2L} \\ i_{\mathrm{pk\_DCM}} = \frac{v_{\mathrm{in}}}{L}\left(M + \sqrt{M^2 + 2Mt_{\mathrm{off}}}\right) \end{cases} \tag{16}$$

where $i_{\mathrm{pk\_CCM}}$ is the peak current in CCM and $i_{\mathrm{pk\_DCM}}$ is the peak current in DCM.

The current limitation for the converter is i_{pkmax}. Then, the inductor current should satisfy

$$\begin{cases} i_{\mathrm{pk\_CCM}} \le i_{\mathrm{pkmax}}, P_o \ge P_{\mathrm{set}} \\ i_{\mathrm{pk\_DCM}} \le i_{\mathrm{pkmax}}, P_o \le P_{\mathrm{set}}. \end{cases} \tag{17}$$

Following the analysis method in the previous section for (16) and (17), it can be concluded that the converter reaches its peak inductor current at full load, and this peak occurs either when the input voltage $v_{\mathrm{in}} = v_{\mathrm{inmax}}$, or at the boundary between DCM and CCM operation. The boundary switching voltage between DCM and CCM will be introduced in the next section. Consequently, the constraints t_4 and t_5 for the t_{OFF} can be expressed as

$$\begin{cases} t_{\mathrm{off}} \le t_4 = \frac{2Li_{\mathrm{pkmax}}\eta v_{\mathrm{inrms}}^2 - 2LP_{o\max}v_{\mathrm{inmax}}}{\eta v_{\mathrm{inrms}}^2(V_o - v_{\mathrm{inmax}})} \\ t_{\mathrm{off}} \le t_5 = \frac{2LP_{o\max}i_{\mathrm{pkmax}}}{2P_{o\max}V_o - \eta v_{\mathrm{inrms}}^2 i_{\mathrm{pkmax}}} \end{cases} \tag{18}$$

where $P_{o\max}$ is the full load power.

D. Selection of the FOT and the Mode Switching Boundary

Combined with the above analysis, the fixed t_{OFF} must satisfy the constraints of the power boundary, peak current, and switching frequency limitations. In combination with (11), (14), and (18), the constraints of the t_{OFF} can be expressed as

$$\max\{t_1, t_2\} \le t_{\mathrm{off}} \le \min\{t_3, t_4, t_5\}. \tag{19}$$

Then the boundary of mode switching for the proposed MCM control strategy can be clearly defined. In ideal MCM operation, the converter's mode-switching boundary voltage is v_b in a half-line cycle. When the $v_{\mathrm{in}} < v_{\mathrm{b}}$, the converter operates in DCM. Conversely, when the $v_{\mathrm{in}} > v_{\mathrm{b}}$, the converter operates in CCM. As the output power increases, the proportion of CCM in a half-line cycle also increases gradually. In combination with (2) to

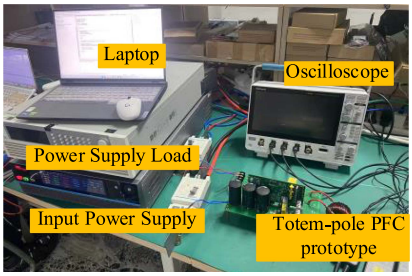

Fig. 7. Experimental environment.

TABLE II
KEY PARAMETERS OF THE TOTEM-POLE PFC PROTOTYPE

Parameters	Values
Input voltage v_{in}	110/220 *V*ac/50 Hz
Output voltage V_o	400 V
Output power P_o	100–1500 W
Power inductor L	150 μH
Output capacitance C_o	2040 μF
Switching frequency f_s	30 kHz–100 kHz

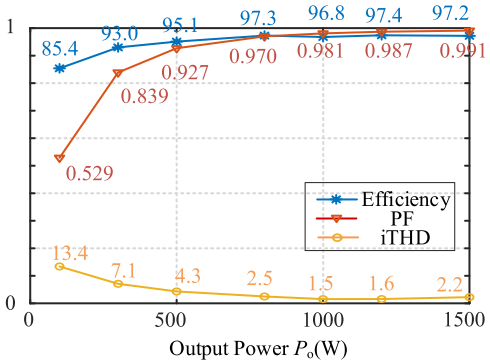

Fig. 8. Performance with average current control in CCM.

(5), the boundary voltage v_b can be expressed as

$$v_b = \frac{\eta v_{\text{inrms}}^2 V_o t_{\text{off}}}{\eta v_{\text{inrms}}^2 t_{\text{off}} + 2P_o L}. \tag{20}$$

IV. EXPERIMENTAL VERIFICATION

To verify the correctness of the theoretical analysis, an experimental platform for the totem-pole PFC converter is established, as shown in Fig. 7. The output power of the converter is 100–1500 W. The key parameters of the totem-pole PFC converter are shown in Table II.

Fig. 8 shows the performance of efficiency and power factor of the totem-pole PFC converter with conventional average current control. As shown in Fig. 8, the efficiency and power factor will decline significantly when the output power is below 500 W. Consequently, the power boundary between DCM and MCM is set to $P_{\text{set}} = 500$ W. The peak current constraint is set to $i_{\text{pkmax}} = 20$ A, with switching frequency limits $f_{\max} = 100$ kHz and $f_{\min} = 30$ kHz. Assuming the input voltage rms value remains constant and the converter efficiency $\eta = 97\%$. According to (19), the constraint of the t_{OFF} under the present circuit parameters is 11.16 μs $< t_{\text{OFF}} <$ 15.46 μs.

The value of L is a critical parameter, influencing both the turn-ON time prediction and the mode-switching boundaries. To improve the system's robustness and reduce the impact of L variations on the controller's performance, the effect of a 10% L tolerance on the constraints of the t_{OFF} is considered. According to (19), the revised constraints of the t_{OFF} is 12.28 μs $< t_{\text{OFF}} <$ 14.59 μs.

To achieve best converter efficiency, we established a loss model of the converter under the proposed MCM control strategy. Theoretical losses, including conduction losses P_{cond}, switching losses P_{sw}, inductance losses P_L, and output capacitor losses P_{ESR}, are considered. By consulting the power device datasheets, the necessary parameters for losses analysis can be obtained. The proposed MCM control is variable-frequency control across the whole operating range. The final losses are derived by integrating the losses of each switching cycle within a half-line cycle. For example, considering switching losses and conduction losses:

In DCM, the current at the turn-ON moment is approximately zero, so the turn-ON losses due to the voltage–current overlap in DCM can be approximately ignored. Only the capacitive loss is considered. Considering the worst case, the energy of the capacitive C_{oss} loss E_c is

$$E_C = \frac{1}{2} C_{\text{oss}} {V_o}^2. \tag{21}$$

The switching loss $\bar{P}_{\text{sw\_CCM}}$ for a single switch cycle in CCM is obtained as follows:

$$\begin{cases} \bar{P}_{\text{onCCM}} = K_1 i_{\text{pk\_CCM}} f_{\text{CCM}} \\ \bar{P}_{\text{offCCM}} = K_2 i_{\text{pk\_CCM}} f_{\text{CCM}} \\ \bar{P}_{\text{CCCM}} = E_C f_{\text{CCM}} \\ \bar{P}_{\text{sw\_CCM}} = \bar{P}_{\text{onCCM}} + \bar{P}_{\text{offCCM}} + \bar{P}_{\text{CCCM}} \end{cases} \tag{22}$$

where K_1 and K_2 are the coefficients for the relationship between the turn-ON and turn-OFF loss energies and current, obtained from the datasheet of the IGBT, $\bar{P}_{\text{onCCM}}$ is the CCM turn-ON loss, $\bar{P}_{\text{offCCM}}$ is the CCM turn-OFF loss, and $\bar{P}_{\text{CCCM}}$ is the CCM capacitive loss.

The switching loss $\bar{P}_{\text{sw\_DCM}}$ for a single switch cycle in DCM is obtained as follows:

$$\begin{cases} \bar{P}_{\text{offDCM}} = K_2 i_{\text{pk\_DCM}} f_{\text{DCM}} \\ \bar{P}_{\text{CDCM}} = E_C f_{\text{DCM}} \\ \bar{P}_{\text{sw\_DCM}} = \bar{P}_{\text{offDCM}} + \bar{P}_{\text{CDCM}} \end{cases} \tag{23}$$

where $\bar{P}_{\text{offDCM}}$ is the DCM turn-OFF loss and $\bar{P}_{\text{CDCM}}$ is the DCM capacitive loss.

From (20), the switching moment t_s between DCM and CCM is obtained as follows:

$$t_s = \frac{\arcsin(v_b)}{\omega} \tag{24}$$

where ω is the angular frequency of the input voltage.

The switching losses of MCM operation can be expressed as

$$P_{\text{sw}} = \frac{4}{T}\left(\int_0^{t_s} \bar{P}_{\text{sw\_DCM}} \mathrm{d}t + \int_{t_s}^{T/4} \bar{P}_{\text{sw\_CCM}} \mathrm{d}t\right). \tag{25}$$

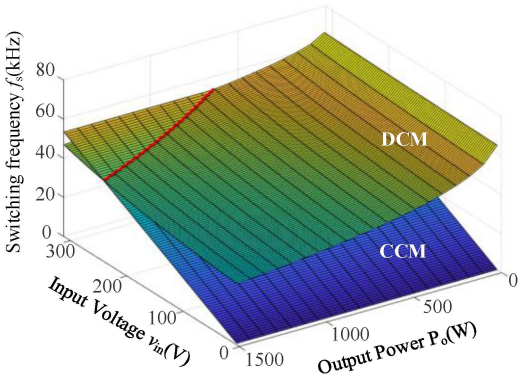

Fig. 9. Full-range switching frequency.

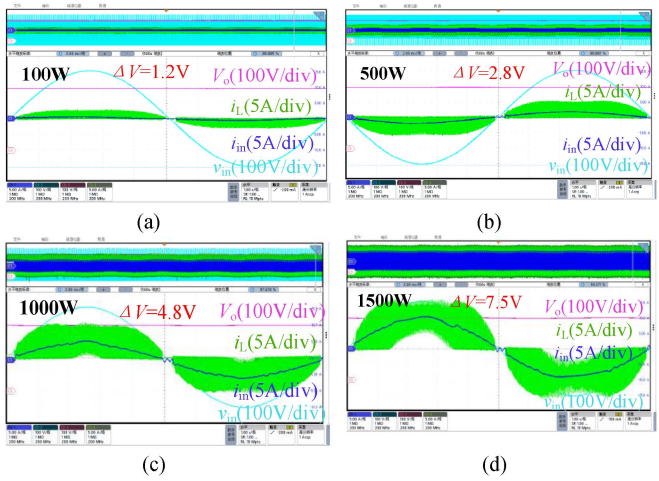

Fig. 10. Operating waveforms at $v_{\rm in} = 220$ V. (a) $P_{\rm o} = 100$ W. (b) $P_{\rm o} = 500$ W. (c) $P_{\rm o} = 1000$ W. (d) $P_{\rm o} = 1500$ W.

During the $t_{\rm ON}$ time, the conduction losses include the conduction losses of the IGBT S_2 and diode D_4. During the t_f time, the conduction losses include the diodes D_1 and D_4. The conduction losses for a single switch cycle in CCM and DCM are obtained as follows:

$$\begin{cases} \bar{P}_{\rm cond\_CCM} = f_{\rm CCM} \\ \left(\int_0^{t_{\rm on}} {\rm V}_F i_L {\rm d}t + \int_0^{t_{\rm on}} {\rm V}_{\rm CE} i_L {\rm d}t + 2\int_0^{t_{\rm off}} {\rm V}_F i_L {\rm d}t\right) \\ \bar{P}_{\rm cond\_DCM} = f_{\rm DCM} \\ \left(\int_0^{t_{\rm on}} {\rm V}_F i_L {\rm d}t + \int_0^{t_{\rm on}} {\rm V}_{\rm CE} i_L {\rm d}t + 2\int_0^{t_f} {\rm V}_F i_L {\rm d}t\right) \end{cases} \tag{26}$$

where $\bar{P}_{\rm cond\_CCM}$ is the CCM conduction loss, $\bar{P}_{\rm cond\_DCM}$ is the DCM conduction loss, V_F is the parallel diode's forward voltage from datasheet, $V_{\rm CE}$ is the collector–emitter voltage of the IGBT from datasheet, and i_L is the inductor current.

The conduction losses of MCM operation can be expressed as

$$P_{\rm cond} = \frac{4}{T}\left(\int_0^{t_s} \bar{P}_{\rm cond\_DCM}{\rm d}t + \int_{t_s}^{T/4} \bar{P}_{\rm cond\_CCM}{\rm d}t\right). \tag{27}$$

Similarly, the other losses of the converter can be estimated. The whole loss analysis formulas are too complex to be presented here, but numerical simulations reveal that the converter operates with lower switching losses in DCM, while the other losses show little difference. Therefore, increasing the proportion of DCM operation can achieve higher efficiency. Based on the previous analysis, the proposed MCM control only changes the mode switching boundary by altering the $t_{\rm OFF}$. Therefore, under the current circuit parameters, a higher efficiency can only be achieved by adjusting the $t_{\rm OFF}$. From (20), the value of $t_{\rm OFF}$ is proportional to the proportion of DCM. Therefore, to improve the converter efficiency, $t_{\rm OFF}$ should be set to the maximum value within the constraints. Finally, the selection FOT is $t_{\rm OFF} = 14.5\ \mu$s.

From (12), the switching frequency curved surfaces of the converter in both CCM and DCM across the entire output range under the current circuit parameters can be obtained, as shown in Fig. 9. The red line is the converter's mode-switching boundary voltage v_b, derived from (20). As shown in Fig. 9, the switching frequency at the mode boundary is continuous, enabling smooth mode switching. For constant output power, the switching frequency is positively correlated with the input voltage under both DCM and CCM, achieving frequency reversal. This verifies the correctness of the theoretical analysis. Under the ideal conditions of the current circuit parameters, the converter's switching frequency ranges from a minimum of 31.4 kHz to a maximum of 66.8 kHz across the full load range, with the power boundary $P_{\rm set} = 637.4$ W, which satisfies system requirements.

Fig. 10 shows the operating waveforms of the totem-pole PFC converter under the proposed control strategy at $P_o = 100 \sim 1500$ W, with $v_{\rm in} = 220$ V. When $P_o < 500$ W, the converter operates in DCM. As the output power increases, the converter transitions to MCM, with the proportion of CCM gradually increasing. As shown in Fig. 10, it can be concluded that the proposed MCM control strategy, based on the FOT, can effectively realize the MCM operation of the converter. The converter operates stably over the full load range, and the output voltage ripple obtains the maximum value of $\Delta V = 7.5$ V at full load, which is about 1.875% of the output voltage.

Based on the previous analysis, the converter operating in DCM or CRM experiences high current stress under high power conditions. CRM is the critical operating state of DCM and can be regarded as the DCM with the least current stress. According to (4), the ideal peak current for the converter operating at $P_o = 1500$ W in CRM is calculated to be 19.28 A. From Fig. 10, it can be seen that when $P_o = 1500$ W, the actual inductor peak current, affected by nonideal factors, is 16.2 A. The MCM control done in this article reduces the peak inductor current by 16.1% at $P_{\rm o} = 1500$ W compared to the ideal CRM control, which will be better compared to the DCM control. This confirms that the proposed control strategy can effectively reduce the current stress of the converter compared to conventional DCM/CRM control strategy.

Fig. 11 shows the operating waveforms of the totem-pole PFC converter under the proposed control strategy at $P_o = 100 \sim 1500$ W, with $v_{\rm in} = 110$ V. Under the current parameters, the boundary power between single DCM and MCM is $P_{\rm set} = 872$

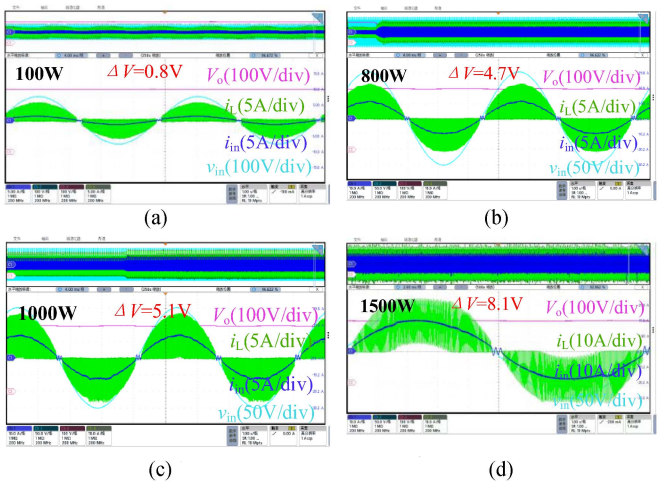

Fig. 11. Operating waveforms at $v_{\text{in}} = 110$ V. (a) $P_{\text{o}} = 100$ W. (b) $P_{\text{o}} = 500$ W. (c) $P_{\text{o}} = 1000$ W. (d) $P_{\text{o}} = 1500$ W.

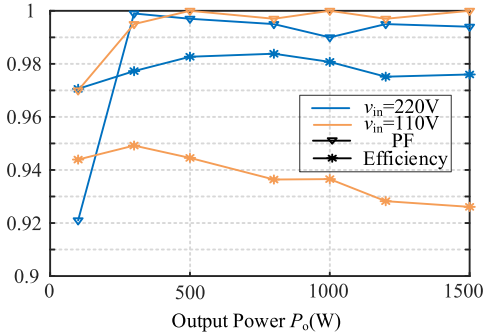

Fig. 12. Measured efficiency and power factor.

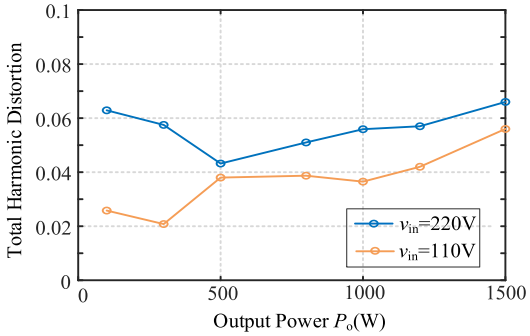

Fig. 13. Measured iTHD.

W. As shown in Fig. 11, the converter achieves stable MCM operation throughout the entire operating range.

Figs. 12 and 13 show the efficiency, PF, and iTHD test comparisons between $v_{\text{in}} = 110$ V and $v_{\text{in}} = 220$ V. As shown in Figs. 12 and 13, the peak efficiency at $v_{\text{in}} = 110$ V and $v_{\text{in}} = 220$ V is 94.9% and 98.3%. The proposed MCM control demonstrates effective PFC with low iTHD under both voltage conditions.

Fig. 14 illustrates the breakdown of losses at $P_o = 300$ and 1500 W, with $v_{\text{in}} = 220$ V. The converter operates in single DCM at 300 W and in MCM at 1500 W. Theoretical efficiencies at 300 and 1500 W are 97.9% and 98.0%, respectively. The

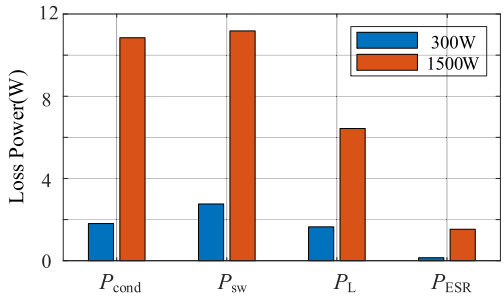

Fig. 14. Breakdown of losses at $P_o = 300$ W and $P_o = 1500$ W.

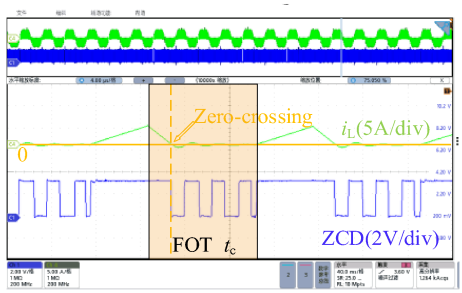

Fig. 15. ZCD signal in DCM.

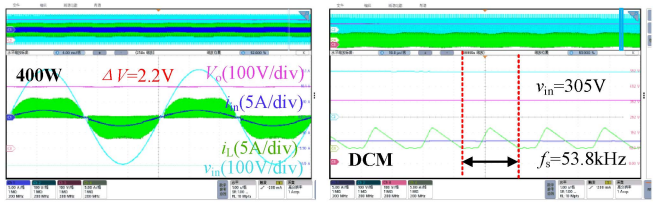

Fig. 16. Operating waveforms in DCM at $P_o = 400$ W. (a) steady state. (b) detail.

measured efficiencies are 97.7% and 97.6%, with efficiency errors all remaining below 0.5%.

Fig. 15 shows the inductor current ZCD waveform in DCM. When the converter operates in DCM, after the inductor current drops to zero, the parasitic capacitances of the high-frequency switches resonate with the power inductor, causing the inductor current to oscillate around zero. As shown in Fig. 15, the ZCD circuit effectively captures the inductor current ZCD signal. Each time the inductor current crosses zero, the ZCD circuit outputs a polarity-reversed signal. By detecting this signal, the present operating mode can be determined, ensuring the correct and stable mode switching.

Fig. 16 shows the steady state and detailed waveforms of the converter single DCM operation at $P_o = 400$ W. The converter output voltage ripple $\Delta V = 2.2$ V, and the converter can still be guaranteed to operate stably in DCM mode at the peak input voltage. Fig. 16(b) shows the detailed waveform of the converter DCM operation when the $v_{\text{in}} = 305$ V and $P_{\text{o}} = 400$ W. At this time, the switching frequency $f_s = 53.8$ kHz. From (12), the theoretical switching frequency $f_s = 54.5$ kHz under the condition can be obtained, and the theory is basically consistent

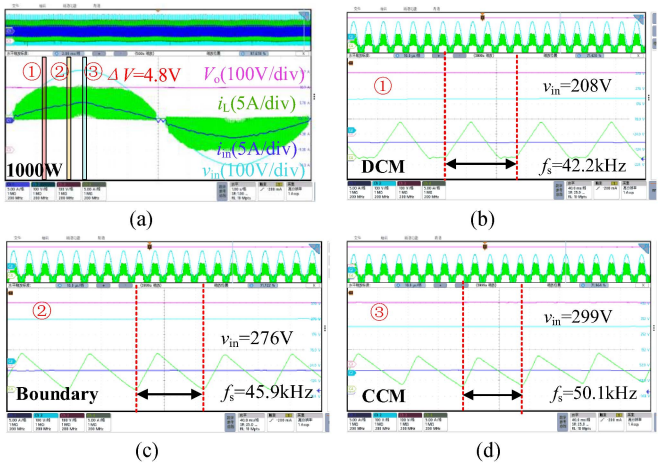

Fig. 17. Operating waveforms in MCM at $P_o = 1000$ W. (a) steady state. (b) DCM detail. (c) boundary detail. (d) CCM detail.

with the reality, with an error of about 1.3%. It confirms the correctness of the analysis in the previous section.

Fig. 17 shows the steady-state and detailed waveforms of the converter operating in MCM at $P_o = 1000$ W. In this figure, region ① represents the converter operating in DCM; region ② represents the boundary between CCM and DCM operation; and region ③ represents the converter operating in CCM. Under this power condition, the converter can achieve stable operation in the MCM mode, with smooth and stable transitions between DCM and CCM. Fig. 17(b) shows the waveform of the converter DCM operation when the $v_{\text{in}} = 208$ V. At this time, the converter switching frequency $f_s = 42.2$ kHz, from (12), the theoretical switching frequency $f_s = 42.6$ kHz, the switching frequency error is about 0.9%. Fig. 17(c) shows the waveform at the CCM/DCM switching boundary. At this time, the input voltage $v_{\text{in}} = 276$ V, and the switching frequency $f_s = 45.9$ kHz. In combination with (12) and (20), the theoretical switching boundary occurs at $v_{\text{in}} = 280.5$ V, $f_s = 46.4$ kHz, and the theory is basically consistent with the reality, the voltage error is about 1.6%. Fig. 17(d) shows the waveform of the converter CCM operation when the $v_{\text{in}} = 299$ V. At this time, the converter switching frequency $f_s = 50.1$ kHz, from (12), the theoretical switching frequency $f_s = 49.8$ kHz, the switching frequency error is about 0.6%. The theory is basically consistent with the reality, and verify the validity of the analysis in the previous section.

Fig. 18 shows the no-load startup waveform of the MCM control strategy developed in this article. At the t_0 moment, the input voltage v_{in} is accessible to the loop. The t_0–t_1 stage represents the precharge stage, during which the input voltage is charged for the output capacitor through the reverse–parallel diode. At the t_1 moment, the precharge is complete, and the precharge circuit is removed from the loop. The t_1–t_2 stage is the reserved dead time. At the t_2 moment, the closed-loop program begins execution, and the output voltage increases continuously until it reaches 430 V at the t_3 moment due to the no-load condition. At the t_3 moment, the converter transitions to burst mode operation, and the output voltage is stabilized at 430 V

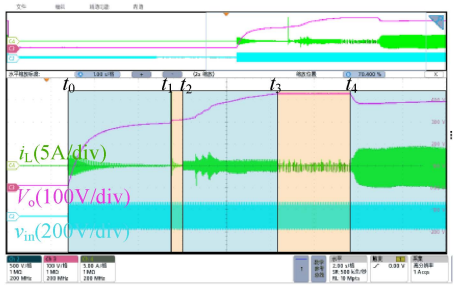

Fig. 18. Waveform of no-load startup.

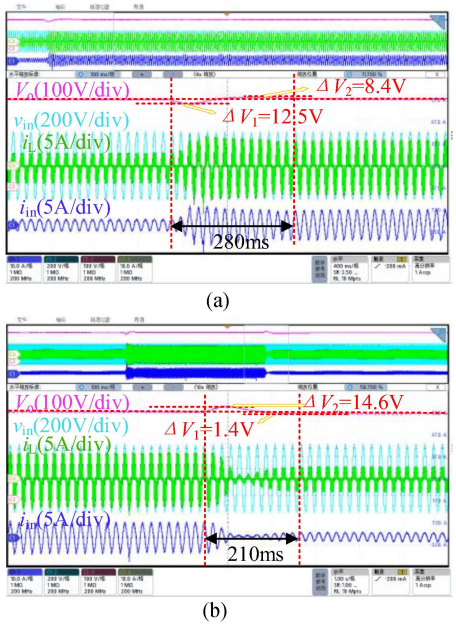

Fig. 19. Operating waveforms of load switching. (a) DCM to MCM. (b) MCM to DCM.

between t_3 and t_4. At the t_4 moment, the converter switches to loaded mode and operates normally.

Fig. 19 shows the load switching test waveforms of the totem-pole PFC converter. Fig. 19(a) shows the converter switching from $P_o = 300$ W in single DCM operation to $P_o = 1000$ W in MCM operation. The dynamic response time of the entire switching process is about 280 ms, and the converter stabilizes after approximately 14 line cycles. The maximum under-regulation voltage during the dynamic response is $\Delta V_1 = 12.5$ V, which is 3.125% of the output voltage. The maximum over-regulation voltage is $\Delta V_2 = 8.4$ V, which is 2.1% of the output voltage. Fig. 19(b) shows the converter switching from $P_o = 1000$ W in MCM operation to $P_o = 300$ W in single DCM operation. The dynamic response time of the entire switching process is about 210 ms, and the converter stabilizes after approximately 10.5 line cycles. The maximum over-regulation voltage is $\Delta V_2 = 14.6$ V, which is 3.65% of the output voltage. The maximum under-regulation voltage during the dynamic response is $\Delta V_1 = 1.4$ V, which is 0.35% of the output voltage. These results confirm that the proposed MCM control strategy effectively maintains a stable output voltage during load switching.

TABLE III
COMPARISON OF MCM CONTROL METHODS

	Proposed MCM	[17]	[14]	[16]	[19]	[13]
Operating mode	DCM/CCM	DCM/CCM	DCM/CCM	DCM/CCM	DCM/CRM	DCM/CCM
Control strategy	FOT based	AVGC based	AVGC and VOT based	AVGC based	UPWC based	Predictive based
Power devices	IGBT(Si)	N/A	MOSFET(Si)	MOSFET(SiC)	GaN	N/A
Power range	100-1500W	50-650W	100-850W	300-3000W	30-320W	300W
Switching frequency	30kHz-70kHz	130kHz	65kHz	65kHz	72kHz-100kHz	100kHz
Peak efficiency	98.3%	N/A	96.5%	99.28%	97.5%	N/A
Light-load efficiency (10% load)	97.2%	N/A	95.6%	98.75%	93.8%	N/A
iTHD(10% load)	6.3%	13%	14%	25.73%	6.2%	4%
Mode-switching boundaries	Clear and controllable	No	No	No	No	No
Control loops	Single voltage loop	One voltage loop, two current loops	One voltage loop, One current loop	One voltage loop, One current loop	Single voltage loop	Single voltage loop
Additional hardware circuitry	Yes	Yes	No	No	No	No
Computational complexity	Single DCM/CCM calculation	No additional calculations	Both the CCM and DCM calculation	Single duty cycle calculation	Both the CRM and DCM calculation	Mode judgment calculation and single DCM/CCM calculation

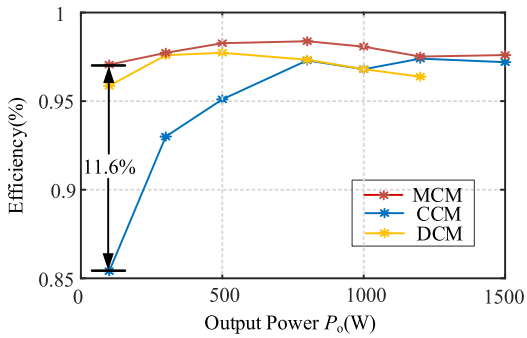

Fig. 20. Measured efficiency.

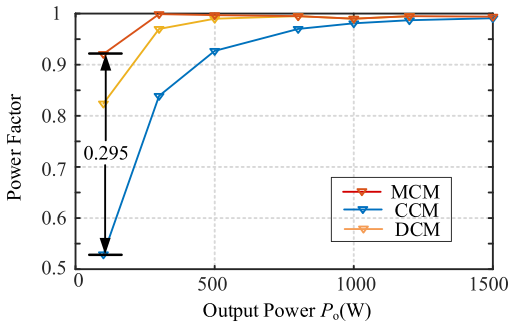

Fig. 21. Measured power factor.

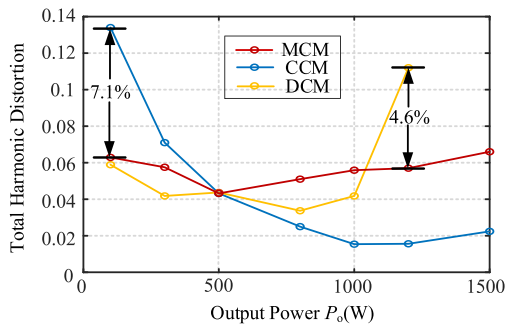

Fig. 22. Measured iTHD.

Figs. 20–22 show the efficiency, power factor, and iTHD test comparisons among the proposed MCM mode control, conventional CCM average current control, and VOT control for DCM, respectively. As shown in Figs. 20 and 21, the peak efficiency of the MCM control strategy is 98.3%, the converter efficiency exceeds 97% across the full load range, and the maximum power factor is 1.000. Compared to the conventional average current control, the converter's performance at light load has significantly improved, with the maximum efficiency increasing by 11.6% at 100 W, the maximum power factor rising by 0.295, and the iTHD decreasing by 7.1%. When $P_o > 1000$ W, the converter begins to enter CCM operation under VOT control. Compared to the VOT control, the converter's performance at heavy load improves significantly, especially in terms of iTHD, with the iTHD decreasing by 4.6% at 1200 W. It is confirmed that the proposed control strategy effectively improves the light-load performance compared to single CCM control and the heavy-load performance compared to single DCM control, enabling efficient and stable operation across a wide load range.

Table III presents a comparison between the proposed MCM control strategy and other recent MCM control strategies. The comparison covers several aspects, including control strategy, power range, efficiency, mode-switching boundary, control loop, additional circuits, and computational complexity. Compared to the existing MCM controls, the proposed MCM control uses silicon-based IGBT devices, which can achieve stable MCM operation with high efficiency, high power factor, and low iTHD across a wide output range of 100–1500 W with lower costs. Furthermore, the proposed MCM control requires lower complexity in both control and computation.

V. CONCLUSION

This article proposes a digital control method for the totem-pole PFC converter operating in MCM, which combines the advantages of single-mode operation to achieve improved performance across a wide load range. First, based on the FOT,

a turn-ON time prediction model for both DCM and CCM is established to unify the control strategies for these modes. By incorporating ZCD, adaptive mode switching is achieved, resolving the complexity issues in existing MCM control strategies. Subsequently, the constraints of the FOT are discussed in terms of the mode-switching power boundary, peak current limitation, and switching frequency limitation.

This discussion identifies the optimal FOT value range and clarifies the mode-switching boundary. Finally, the effectiveness and accuracy of the proposed control strategy are validated through prototype testing. The experimental results demonstrate that the proposed control strategy enables stable MCM operation in the totem-pole PFC converter. The peak efficiency of the experimental prototype is 98.3%, with a maximum power factor of 1.000. Compared to the conventional DCM/CRM control strategy, the proposed method effectively reduces converter current stress, with peak inductor current decreased by up to 16.1%. When compared to the conventional CCM control strategy, it significantly enhances light-load performance, improving efficiency by up to 11.6%, increasing power factor by 0.295 and the iTHD decreasing by 7.1%.

REFERENCES

[1] C.-W. Lin, H.-J. Chiu, M.-S. Tzeng, J.-W. Yeh, and C.-H. Huang, "Novel bidirectional on-board charger for G2V and V2X applications on wide-range batteries," *IEEE J. Emerg. Sel. Top. Power Electron.*, vol. 12, no. 2, pp. 2292–2305, Apr. 2024.

[2] J.-S. Kim, T. Kim, J. Bae, J.-K. Han, and G.-W. Moon, "A hybrid current reference control method for PFC converter in server power supply," *IEEE Trans. Power Electron.*, vol. 39, no. 1, pp. 64–70, Jan. 2024.

[3] T.-T. Le, J. Lee, and S. Choi, "Single-stage totem-pole AC–DC converter based on boost half-bridge structure for battery chargers," *IEEE Trans. Power Electron.*, vol. 39, no. 1, pp. 1060–1073, Jan. 2024.

[4] Q. Huang and A. Q. Huang, "Review of GaN totem-pole bridgeless PFC," *CPSS Trans. Power Electron. Appl.*, vol. 2, no. 3, pp. 187–196, Sep. 2017.

[5] K. De Gusseme, D. M. Van de Sype, A. P. M. Van den Bossche, and J. A. Melkebeek, "Input-current distortion of CCM boost PFC converters operated in DCM," *IEEE Trans. Ind. Electron.*, vol. 54, no. 2, pp. 858–865, Apr. 2007.

[6] C. Zhao and X. Wu, "Accurate operating analysis of boundary mode totem-pole boost PFC converter considering the reverse recovery of MOSFET," *IEEE Trans. Power Electron.*, vol. 33, no. 12, pp. 10038–10043, Dec. 2018.

[7] Q. Huang, R. Yu, Q. Ma, and A. Q. Huang, "Predictive ZVS control with improved ZVS time margin and limited variable frequency range for a 99% efficient, 130-W/in^3 MHz GaN totem-pole PFC rectifier," *IEEE Trans. Power Electron.*, vol. 34, no. 7, pp. 7079–7091, Jul. 2019.

[8] K. D. Gusseme, D. M. V. Sype, A. P. M. Van den Bossche, and J. A. Melkebeek, "Digitally controlled boost power-factor-correction converters operating in both continuous and discontinuous conduction mode," *IEEE Trans. Ind. Electron.*, vol. 52, no. 1, pp. 88–97, Feb. 2005.

[9] S. F. Lim and A. M. Khambadkone, "A simple digital DCM control scheme for boost PFC operating in both CCM and DCM," *IEEE Trans. Ind. Appl.*, vol. 47, no. 4, pp. 1802–1812, Jul./Aug. 2011.

[10] L. Wang, Q. H. Wu, W. H. Tang, Z. Y. Yu, and W. Ma, "CCM-DCM average current control for both continuous and discontinuous conduction modes boost PFC converters," in *Proc. IEEE Elect. Power Energy Conf.*, 2017, pp. 1–6.

[11] W.-H. Wang and Y.-Y. Tzou, "Using repetitive control for light load THD and efficiency improvement for boost digital PFC converters," in *Proc. 7th Int. Power Electron. Motion Control Conf.*, 2012, pp. 1915–1920.

[12] W.-S. Wang and Y.-Y. Tzou, "Light load efficiency improvement for AC/DC boost PFC converters by digital multi-mode control method," in *Proc. IEEE 9th Int. Conf. Power Electron. Drive Syst.*, 2011, pp. 1025–1030.

[13] H. S. Nair and N. L. Narasamma, "An improved digital algorithm for boost PFC converter operating in mixed conduction mode," *IEEE J. Emerg. Sel. Top. Power Electron.*, vol. 8, no. 4, pp. 4235–4245, Dec. 2020.

[14] Z. Chen, J. Xu, P. Davari, and H. Wang, "A mixed conduction mode-controlled bridgeless boost PFC converter and its mission profile-based reliability analysis," *IEEE Trans. Power Electron.*, vol. 37, no. 8, pp. 9674–9686, Aug. 2022.

[15] Y.-S. Lai, X.-Y. Wu, and Y.-Y. Huang, "Novel continuous transition of CCM and DCM switching control method for efficiency improvement of PFC," in *Proc. IEEE Int. Future Energy Electron. Conf.*, 2023, pp. 29–33.

[16] Y.-S. Lai, X.-Y. Wu, and Y.-Y. Huang, "New seamless switching control technique between CCM and DCM for boost PFC without additional zero crossing point sensing circuit," *IEEE Trans. Ind. Electron.*, vol. 71, no. 10, pp. 12100–12110, Oct. 2024.

[17] C. W. Clark, F. Musavi, and W. Eberle, "Digital DCM detection and mixed conduction mode control for boost PFC converters," *IEEE Trans. Power Electron.*, vol. 29, no. 1, pp. 347–355, Jan. 2014.

[18] R. Fernandes and O. Trescases, "A multimode 1-MHz PFC front end with digital peak current modulation," *IEEE Trans. Power Electron.*, vol. 31, no. 8, pp. 5694–5708, Aug. 2016.

[19] R. Min, G. Shen, Q. Tong, Q. Zhang, H. Peng, and X. Zou, "Unified pulse-width-cycle control strategy to achieve mixed DCM/CRM operation and consistent valley switching for boost PFC converter," *IEEE Trans. Power Electron.*, vol. 36, no. 11, pp. 13304–13316, Nov. 2021.

[20] X. Ren, Z. Guo, Y. Wu, Z. Zhang, and Q. Chen, "Adaptive LUT-based variable on-time control for CRM boost PFC converters," *IEEE Trans. Power Electron.*, vol. 33, no. 9, pp. 8123–8136, Sep. 2018.

[21] X. Zhang, J. Xu, B. Bao, and G. Zhou, "Asynchronous-switching map-based stability effects of circuit parameters in fixed off-time controlled buck converter," *IEEE Trans. Power Electron.*, vol. 31, no. 9, pp. 6686–6697, Sep. 2016.

[22] Z. Zhang, J. Zhang, and S. Shao, "A variable off-time control method for a single-phase DCM microinverter," *IEEE Trans. Power Electron.*, vol. 33, no. 8, pp. 7229–7239, Aug. 2018.

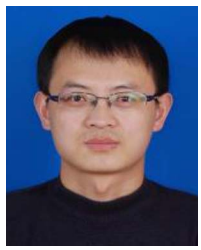

Fangang Meng (Member, IEEE) received the B.S. degree in thermal energy and power engineering, and the M.S. and Ph.D. degrees in electrical engineering from the Harbin Institute of Technology, Harbin, China, in 2005, 2007, and 2011, respectively.

Since 2020, he has been working as a Professor with the Harbin Institute of Technology, Weihai, China. His research interests include harmonic detection, stability analysis of converter, and high-power rectifier.

Yuan Shu received the B.S. degree in electrical engineering from the Harbin Institute of Technology, Harbin, China, in 2021. He is currently working toward the M.S. degree in electrical engineering with the Harbin Institute of Technology, Weihai, China.

His research interests include active power factor correction, rectifiers, and resonant converters.

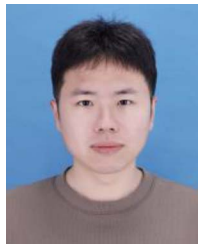

Jinmeng Wu (Graduate Student Member, IEEE) received the B.S. degree in electrical engineering from the Harbin University of Science and Technology, Harbin, China, in 2018, and the M.S. degree in electrical power engineering from the Taiyuan University of Technology, Taiyuan, China, in 2021. He is currently working toward the Ph.D. degree in electrical engineering with the Harbin Institute of Technology, Harbin, China.

His research interests include bidirectional ac–dc converters and multistage converter stability analysis.

Shengren Yong received the B.S. degree in electrical engineering from the Northeast Agricultural University, Harbin, China, in 2023. He is currently working toward the M.S. degree in electrical engineering with the Harbin Institute of Technology, Harbin, China.

His research interests include the design methods and control strategies of bidirectional dc–dc converters and high-efficiency power.

Yufeng Chen received the B.S. degree in electrical engineering from the Wuhan University, Wuhan, China, in 2024. He is currently working toward the M.S. degree in electrical engineering with the Harbin Institute of Technology, Weihai, China.

His research interests include bidirectional ac–dc converters and rectifier.